

5 MeV BEAM DIAGNOSTICS AT THE MAINZ ENERGY-RECOVERING SUPERCONDUCTING ACCELERATOR MESA

S. Heidrich *, K. Aulenbacher, Institute of Nuclear Physics, Mainz, Germany

Abstract

Within the next few years, a new energy-recovering superconducting electron accelerator will be built at the Institute of Nuclear Physics in Mainz. For injection into the main accelerator the beam parameters need to be known. This requires a high resolution longitudinal beam diagnostic system at the 5 MeV-injection arc. The system employs two 90° vertical deflection dipoles, which aims to achieve an energy resolution of 240 eV and a phase resolution of 46 μm.

As a second challenge, the transverse emittance measurements will take place at full beam current. This demands an extremely heat resistant diagnostic system, realised by a method similar to flying wire.

MAINZ ENERGY-RECOVERING SUPERCONDUCTING ACCELERATOR

The Mainz Energy-recovering Superconducting Accelerator MESA will run in two different beam modes. The energy recovering mode allows beam currents up to 1 mA at a maximum beam energy of 105 MeV, while the external beam mode achieves an energy of 155 MeV but limits the maximum current to 150 μA. The part of the beam diagnostics discussed in this article will be installed downstream of the normal-conducting pre-accelerator at 5 MeV. Here, the beam will have a normalized transverse emittance of about 1 μm, an energy spread in the order of 2 keV and a bunch length of about 240 μm. For the second stage of MESA, 10 mA beam current is envisaged. The preinjector MAMBO (Milliamperere Booster) is already designed for this average current. [1]

LONGITUDINAL BEAM DIAGNOSTICS

The design of the longitudinal beam diagnostic combines a magnetic energy spectrometer with a dipole cavity for bunch length measurements. A set-up sketch of the system is displayed in Figure 1. First, the beam is guided through a 90° deflection dipole which causes a transverse spread depending on the energy distribution of the beam. By then collimating the dispersed beam through a 100 μm-gap, an energy window of ±240 eV is cut out. As displayed in Figure 2, the beam shows a large phase dispersion caused by the R₅₁ element of the dipole transformation matrix at this point. This phase smearing compromises the subsequent bunch length measurement and needs to be compensated with an additional quadrupole directly behind the collimator and a second 90° dipole. By that, the energy measurement system becomes achromatic and the phase smearing vanishes.

Then, the energy collimated beam is guided to the phase measurement system which consists of a focusing quadrupole, a 500 W 1.3 GHz dipole cavity, a defocusing quadrupole and a tungsten wire which cuts out a 60 μm long part of the bunch. The radiation caused by the interaction between the beam and the wire is proportional to the integrated current of the selected phase space and is measured with a scintillation detector. To scan the whole longitudinal phase space, the phase of the dipole cavity is shifted and the beam is steered over the energy collimator. To compensate the influence of the steerer on the R₅₁ matrix element, a second steerer has to be employed downstream of the energy collimator.

The measured phase space can be displayed in real time with a repetition rate of 10 Hz.

Contrary to the transverse diagnostics it is not possible to operate at full beam current. Instead, a pulsed or single bunch mode needs to be implemented.

It has to be mentioned that the energy spectrometer deflects the beam vertically while the injection arc has a horizontal set up. However, it may be assumed that the longitudinal phase space does not depend on the observation direction.

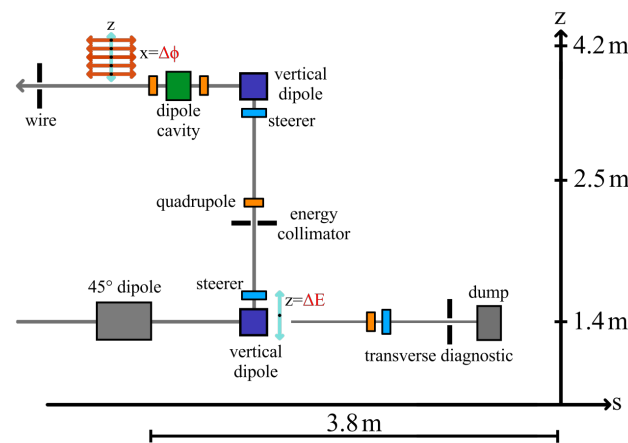


Figure 1: The longitudinal beam diagnostic consists of a vertically deflecting 90° energy spectrometer with subsequent chromatic correction and a dipole cavity which is used to measure the extension of the beamlets.

* s.heidrich@uni-mainz.de

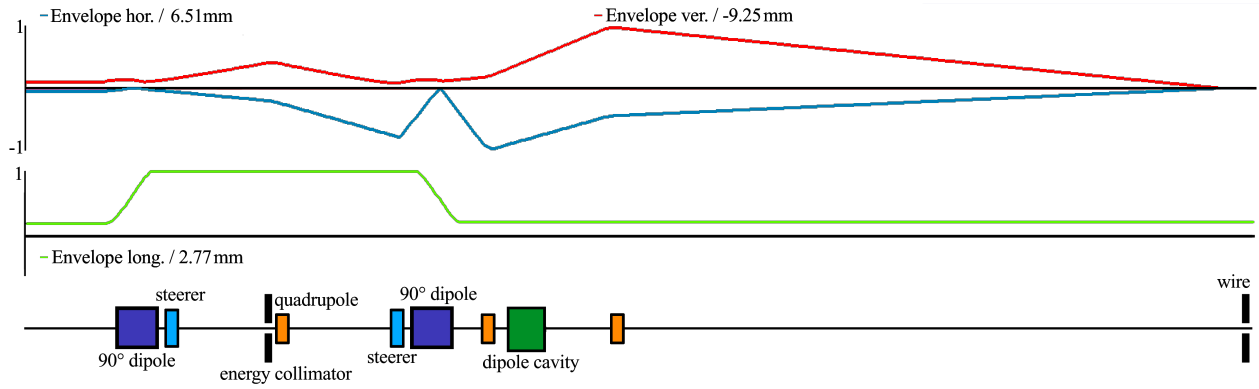


Figure 2: The transverse and longitudinal beam envelopes are displayed for the longitudinal diagnostic system. Phase smearing increases the size of the longitudinal envelope from 0.6 mm to 2.77 mm downstream of the first 90° dipole. Using a second identical dipole allows to correct this behaviour, so that the energy spectrometry does not influence the following phase measurement. Before entering the dipole cavity, both transverse envelopes rise to several millimeters, which calls for examination of nonlinear contributions in the cavity and the quadrupoles.

The resolution r_ϕ of the phase measurement system is given by

$$r_\phi = \pm \frac{c}{\omega_{rf}} \times \arcsin\left(\frac{\sigma_x}{R_{12} \tan(\alpha_0)}\right) \quad (1)$$

with [2]

$$\alpha_0 = 1.46 \times 10^{-3} \text{ mrad} \sqrt{Q_0 P_{rf}}. \quad (2)$$

Here, c is the speed of light, ω_{rf} is the circular frequency of the cavity, σ_x equals the size of the focused beam spot, R_{12} describes the corresponding element of the beam transformation matrix behind the cavity, α_0 is the angular amplitude of the cavity kick, Q_0 is the quality of the cavity (typically around 10000) and P_{rf} stands for the available RF Power.

For the MESA set-up, the RF power available for diagnostics is limited to 500 W. An increase would involve high costs and tough requirements for the cooling system of the cavity.

Since the phase measurement lies 2.4 m above the pre-accelerator, the achievable drift length can be set to 6 m without interfering with any other components. To further increase the phase resolution, two quadrupoles are implemented adjacent to the cavity. They are able to focus the beam on the detector wire while magnifying the kick of the cavity by a factor of 1.77. This is done by setting R_{12} to 12.36 m.

In this first order calculation, the achievable beam size is $\sigma_x = 50 \mu\text{m}$ and the circular frequency is $\omega_{hf} = 2\pi \times 1.3 \text{ GHz}$. Inserting those values into equation (1) gives a resolution of $r_\phi = \pm 45.6 \mu\text{m}$.

TRANSVERSE BEAM DIAGNOSTICS

To scan the transverse beam profile, the beam is steered over a fixed tungsten wire with $10 \mu\text{m}$ radius. The resulting radiation is proportional to the integrated beam current and can easily be measured by a scintillation detector behind

the wire. In combination with an additional quadrupole, the profile measurements can then be utilized to determine the emittance of the beam [3].

To ensure that the diagnostic wire does not melt during irradiation, it is necessary to evaluate the deposited heat load for a maximum current of 1 mA. Therefore, the set-up was simulated with *FLUKA* [4] [5] for a strongly focused beam with a radius of $10 \mu\text{m}$. The resulting power deposition reaches a maximum of about $4.6 \text{ GW mm}^{-3} \text{ A}^{-1}$. Under the assumption that the cooling only takes place by black body radiation, the temperature of the wire can be calculated by solving equation (3). Here, P is the deposited power density, Q defines the specific heat capacity of tungsten, R is the wire radius, ρ stands for the material density, T equals the temperature, ϵ is the emissivity and k_B is the Boltzmann constant.

$$\dot{T} = \frac{P}{Q\rho} - \frac{2\epsilon k_B}{Q\rho R} (T^4 - T_0^4) \quad (3)$$

The melting point of the wire would then be reached within $1 \mu\text{s}$. Consequently, the beam is steered over the wire for just one 1 kHz cycle by a fast ferrite magnet and is then allowed to cool down for a few seconds before running the next measurement.

It is expected that the dumping of the beam directly downstream of the diagnostic wire will lead to a large amount of background radiation. To evaluate the signal to noise ratio r_{sn} , the shielded set-up was simulated with *FLUKA* for two cases. Case a: The diagnostic wire is exposed to the beam; Case b: The wire is excluded. Since the signal to noise ratio will be reduced when the beam size is increased, a large beam size of $\sigma_x = 1 \text{ mm}$ was simulated for a tungsten wire with the radius $R = 10 \mu\text{m}$. The simulation results are displayed

in Figure 3. For case a, the amount of deposited energy in the detector per incoming electron is $E_a = 3579(10)$ eV, for case b it is $E_b = 44(8)$ eV. This leads to a signal to noise ratio of

$$r_{sn} = \frac{E_a - E_b}{E_b} = 80.3 \pm 10. \quad (4)$$

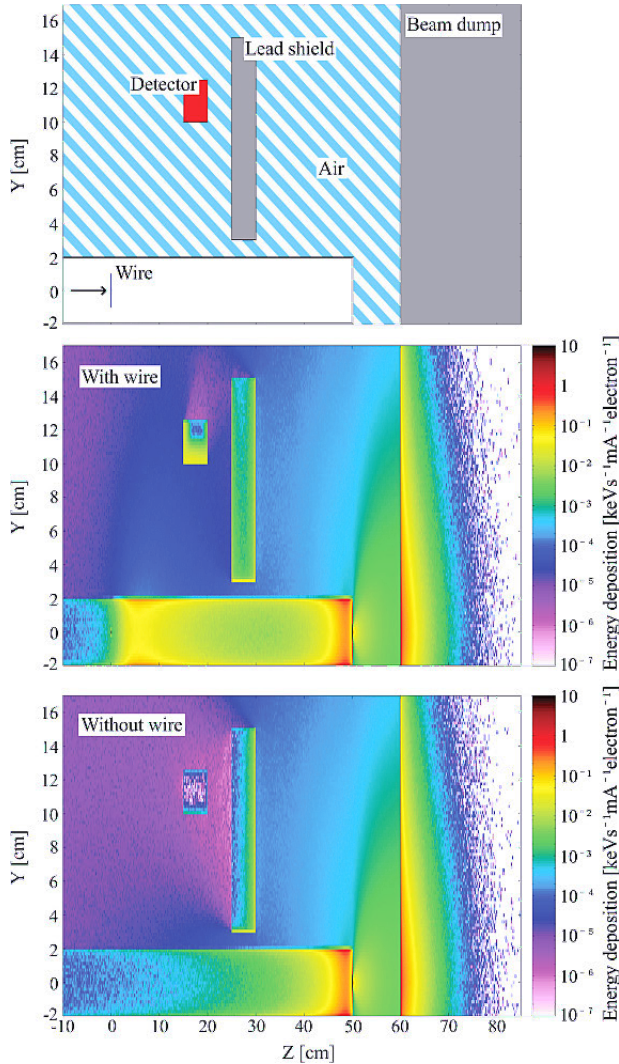


Figure 3: The influence of the background radiation was evaluated by simulating the detector set-up with and without the diagnostic wire. The results show that the energy deposition in the detector drops by two magnitudes when the diagnostic wire is excluded.

Without further post-processing, the measurements of the beam size are limited in their precision by the diameter of the wire.

In the following, a procedure is described that aims to compensate the wire size and consists of three steps:

Step 1 The produced radiation strongly depends on the radial distance of an impacting electron to the axis of the wire. Thus, the signal response to different impact points needs to be evaluated. Intuitively it could be assumed that the signal intensity would only depend on the path-length of the electron through the target, which is given by the thickness of the wire at the respective position. However, this assumption does not match the simulation results of several point-like impact areas on a tungsten wire with the radius $R = 15 \mu\text{m}$, which are displayed in Figure 4. Most likely, this discrepancy is caused by multi scattering processes and needs to be further investigated. In a first approach, the data was fitted with a high order polynomial function $w(x) = a - kx^{10}$, which in the following will be used as the weighting function of the wire.

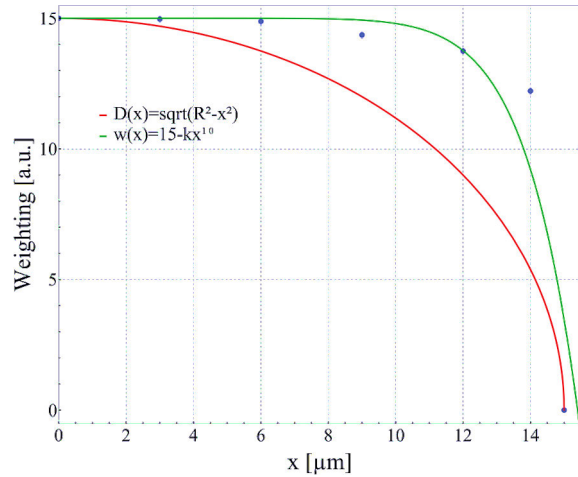


Figure 4: The dependency of the wire signal on the position of point-like impact areas was simulated to evaluate the weighting function. The results show that the height of the signal is not proportional to the thickness $D(x)$ of the wire at the position of the impact point. For further calculations, a high order polynomial fit was used.

Step 2 With the weighting function, a measurement of the beam profile can be simulated.

Equation (5) gives the wire signal intensity depending on the position of the wire axis in relation to the center of the beam ($x = x_0 = 0$).

$$I_{\text{meas}}(x_0) = \int_0^{\Delta t} \tau(t) dt \int_{x_0-R+x(t)}^{x_0+R+x(t)} J(x) \times w(x) dx. \quad (5)$$

Here, Δt is the time resolution of the detector, R defines the radius of the wire and $\tau(t)$ equals the temporal weighting function of the detector, which is assumed to be constant. $J(x)$ is the density distribution of the beam profile and assumed to be gaussian. If the beam profile is not gaussian, $J(x)$ needs to be replaced accordingly.

To simulate a measurement, the beam size of interest and a list of wire positions is initially set and then processed

with equation (5). Figure 5 shows the simulation results for a beam size of $\sigma_x = 10 \mu\text{m}$ at 31 equidistant wire positions and a wire radius of $R = 15 \mu\text{m}$. In this case, the measurement would overestimate the true beam size by 27.5%.

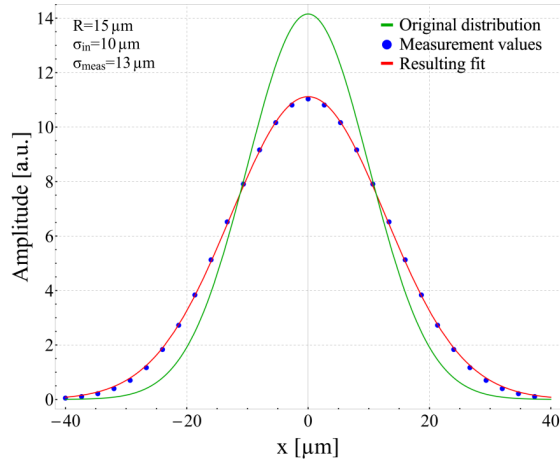


Figure 5: By using the calculated weighting function, a single wire measurement can be simulated. The ratio of the resulting "measured" beam size σ_{meas} to the initial "true" beam size σ_{in} then gives the correction factor of the measurement.

Step 3 The results of a real measurement can be processed by repeating step 2 for every beam size of interest. Figure 6 shows the correction factors of 20 simulations from $\sigma_x = 10 \mu\text{m}$ to $\sigma_x = 50 \mu\text{m}$. By employing the resulting correction curve on the list of measured beam sizes, the influence of the wire thickness can be compensated.

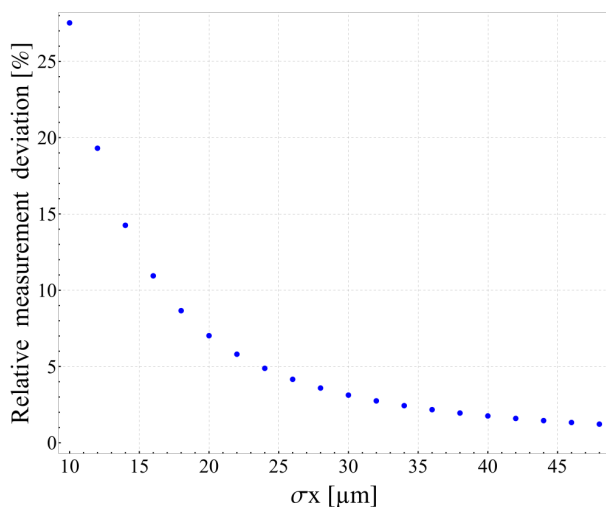


Figure 6: The correction factors depend on the material and the diameter of the diagnostic wire as well as on the beam size. The displayed values are the results for a tungsten wire with a radius of $15 \mu\text{m}$. In this case, the measurement of the beam profile results in an overestimation of up to 27.5% for a minimum beam size of $10 \mu\text{m}$.

ISBN 978-3-95450-177-9

OUTLOOK

Except the 90° dipole magnets all discussed systems are in a preliminary design status and will be built within the next two years.

There are concerns about the influence of the second order transformation matrix elements on the longitudinal diagnostics. They may lead to additional phase smearing, which needs to be further investigated.

For full current beam profile measurements, an appropriate beam dump needs to be designed to withstand a maximum beam power of 50 kW.

The compensation procedure of the wire size for transverse beam profile measurements assumes a gaussian beam profile, which especially for high current densities may not be true. Additionally any roughness or bending of the wire is neglected. These issues needs to be further investigated with an experimental set up under real conditions.

CONCLUSION

The working principles of a longitudinal and transverse beam diagnostic system for MESA at 5 MeV were discussed. It was shown that the longitudinal diagnostics could provide an energy resolution of 240 eV and a phase resolution of $46 \mu\text{m}$.

The described transverse system could be used to perform full current beam profile measurements. A procedure to calculate correction factors for the influence of the diameter of the diagnostic wire may lead to an optimization of the achievable resolution.

ACKNOWLEDGEMENTS

The work at the injection arc and the beam diagnostics of MESA is supported by the **DFG** (Deutsche Forschungsgemeinschaft) through the excellence cluster **PRISMA** (Precision Physics, Fundamental Interactions and Structure of Matter).

REFERENCES

- [1] R.Heine, K. Aulenbacher, "MESA - Sketch of an Energy Recovering Linac for Nuclear Physics Experiments at Mainz", Proceedings of IPAC2012, New Orleans, Louisiana, USA (2012).
- [2] K.W. Nilles, "Master thesis: Die Apparatur zur schnellen Diagnostik des longitudinalen Phasenraumes am Injektorlinac des Mainzer Mikrotrons", MAMI, Mainz, Germany (1989).
- [3] H. Wiedemann "Particle Accelerator Physics Third Edition", Springer (2007), doi:10.1007/s12541-016-0037-5
- [4] A. Ferrari, P.R. Sala, A. Fassò, and J. Ranft "FLUKA: a multi-particle transport code", CERN-2005-10 (2005), INFN/ TC_05/11, SLAC-R-773.
- [5] T.T. Böhlen, F. Cerutti, M.P.W. Chin, A. Fassò, A. Ferrari, P.G. Ortega, A. Mairani, P.R. Sala, G. Smirnov, V. Vlachoudis "The FLUKA Code: Developments and Challenges for High Energy and Medical Applications", Nuclear Data Sheets 120, 211-214 (2014).